No consistent simulated trends in the Atlantic Meridional Overturning Circulation for the past 6,000 years

Zhiyi Jiang[1], Chris M. Brierley[1], Jürgen Bader[2*], Pascale Braconnot[3*], Michael Erb[4*], Peter O. Hopcroft[5*], Dabang Jiang[6*], Johann Jungclaus[2*], Vyacheslav Khon[7*,8*], Gerrit Lohmann[9*], Olivier Marti[3*], Matthew B. Osman[10*], Bette Otto-Bliesner[11*], Birgit Schneider[12*], Xiaoxu Shi[9*], David J. R. Thornalley[1*], Zhiping Tian[6*]and Qiong Zhang[13*,14*]

[1]Department of Geography, University College London, London, WC1E 6BT, UK
[2]Max-Planck-Institut für Meteorologie, Hamburg, Germany
[3]Laboratoire des Sciences du Climat et de l'Environnement-IPSL, Gif-sur-Yvette, France
[4]School of Earth and Sustainability, Northern Arizona University, Flagstaff, AZ, USA
[5]School of Geography, Earth and Environmental Sciences, University of Birmingham, B15 2TT, UK
[6]Institute of Atmospheric Physics, Chinese Academy of Sciences, Beijing, China
[7]Lyell Centre, Heriot-Watt University, Edinburgh, United Kingdom
[8]A. M. Obukhov Institute of Atmospheric Physics, Russian Academy of Sciences, Moscow, Russia
[9]Alfred-Wegener-Institut Helmholtz-Zentrum für Polar- und Meeresforschung, Bremerhaven, Germany
[10]Department of Geosciences, University of Arizona, Tucson, Arizona, USA
[11]National Center for Atmospheric Research (NCAR), Boulder, CO, USA
[12]Institute of Geosciences, Kiel University, Kiel, Germany
[13]Department of Physical Geography, Stockholm University, Stockholm, Sweden
[14]Bolin Centre for Climate Research, Stockholm University, Stockholm, Sweden
[*]These authors are listed in alphabetical order

Key Points:

- A multi-model ensemble of Holocene transient simulations by general circulation models is emerging
- It suggests that neither the overall AMOC strength, nor its variability, changed during the mid-to-late Holocene
- This lack of overall change is consistent with available proxy reconstructions

Corresponding author: Zhiyi Jiang, z.jiang.17@ucl.ac.uk

Abstract

The Atlantic Meridional Overturning Circulation (AMOC) is a key feature of the North Atlantic with global ocean impacts. The AMOC's response to past changes in forcings during the Holocene provides important context for the coming centuries. Here, we investigate AMOC trends using an emerging set of transient simulations using multiple global climate models for the past 6,000 years. We find no consistent changes in the overall AMOC strength across the simulations, which conforms with reconstructions assimilating proxy records. Similarly, the decadal variability of the AMOC does not change during the mid- and late-Holocene. There are interesting AMOC changes seen in the early Holocene, but their nature depends a lot on which inputs are used to drive the experiment.

Plain Language Summary

The Atlantic Meridional Overturning Circulation (AMOC) is a deep ocean circulation system that is both important for climate and vulnerable to climate changes. Here we use a set of multiple climate models to look at how the AMOC responded to changes in climate drivers over the past few thousand years. The changes are only small in all of the models, and do not always agree in direction. The AMOC naturally varies on decadal timescales, but we do not see any strong trends in its variability either. These results fit with recent data reconstructions suggesting that the models are reasonable in their representation of the Holocene AMOC.

1 Introduction

The Atlantic Meridional Overturning Circulation (AMOC; Rahmstorf, 2006) is a large-scale ocean circulation that helps transport heat poleward moderating the climate of Europe and eastern North America (Cherchi, 2019). Direct observations of it only became available in 21^{st} century, and show a noticeable weakening (Smeed et al., 2018) that is not captured by climate models (Weijer et al., 2020). Despite this inconsistency, the IPCC Assessment Report 6 (AR6) projects a further weakening in AMOC strength with high confidence (Fox-Kemper et al., 2021), although the magnitude remains uncertain. Evaluating the response of models to past variations in boundary conditions (such as orbital configuration and greenhouse gases levels, ice sheet extent) against proxy-derived reconstructions of the AMOC can potentially help constrain the uncertainty in future projections (Kageyama et al., 2018).

The Holocene Epoch (roughly the past 12,000 years) saw gradual changes in the seasonal cycle of incoming solar radiation due to the changes in the orbital configuration (Braconnot et al., 2019; Otto-Bliesner et al., 2017). There were also decreasing greenhouse gases (GHG; CO_2, CH_4 and N_2O) concentrations, followed by an gradual increase until industrialisation (Tian et al., 2022; He, 2011). The decaying ice-sheets released meltwater throughout the early Holocene (Peltier et al., 2015; Argus et al., 2014), with an abrupt release into the Labrador Sea during the 8.2 ka event (Aguiar et al., 2021). Reconstructions also show variations in anthropogenic land-use, total solar irradiance (Vieira et al., 2011), and volcanic activity (Kobashi et al., 2017) that was particularly strong at 8.6-8 ka BP and 7.5-7 ka BP.

Proxy reconstructions of Holocene AMOC and its deep water components argue for a range of long-term changes. Those that provide information on the overall integrated AMOC all suggest a slightly weaker early Holocene AMOC. For the mid to late Holocene behaviour they can be split into two main groups. Reconstructions from the Florida Straits (Lynch-Stieglitz et al., 2009) or based on Pa/Th ratios (e.g Ng et al., 2018; Lippold et al., 2019; Hoffmann et al., 2018) suggest little change in AMOC strength since 9,000 years ago. Conversely, reconstructions based on SST fingerprints and changes in seawater Cd concentration suggest a gradual overall decline in AMOC from the mid to late Holocene (Ayache et al., 2018; Valley et al., 2022). Data assimilation approaches also suggest little long-term AMOC change in the Holocene (Ritz et al., 2013; Osman et al., 2021).

Snapshot equilibrium simulations for 6,000 years ago (6 ka) have been performed for the *midHolocene* experiment of the Palaeoclimate Modelling Intercomparsion Project (PMIP; Kageyama et al., 2018). Brierley et al. (2020) find that the AMOC strength in the *mid-Holocene* ensemble is not markedly different. These results are supported by associated simulations of the last interglacial (Jiang et al., 2023). There is known to a resolution dependency (Shi & Lohmann, 2016; Shi et al., 2020), which itself could vary by model (Jackson et al., 2020).

Currently there is an effort in the community to undertake transient Holocene simulations, which focus on analysing the time-dependent interactions between different components in the Earth system and the long-term climate evolution. Here we collate the emerging set of Holocene transient simulations from different modelling groups to further investigate whether there is a consistent message from the ensemble about trends in (i) AMOC strength, (ii) its spatial structure and (iii) its internal/decadal variability since 6,000 years ago. Summary information about the different transient simulations is given in Section 2, along with an explanation of the analysis procedures. Further information about each of the individual simulations can be found in the supplemental material. The results of the AMOC trends in Holocene transient runs are presented in Section 3, followed by discussion and conclusions in the last section.

2 Data and methods

We use nine transient model simulations from eight different coupled climate models (summarised in Table 1). All of the simulations are run continuously towards the present day from 6ka or earlier. Not all of the models are truly independent: EC-Earth3-veg-LR, KCM, and IPSL-CM5 use NEMO ocean model NEMO at different resolutions (Madec et al., 2008; Crosta et al., 2018); AWI-ESM-2, MPI-ESM, and KCM have versions of the ECHAM atmosphere (Shi et al., 2020; Sidorenko et al., 2019; Mauritsen et al., 2019; Roeckner et al., 2003).

All simulations incorporate changes in the orbital configuration, and their associated changes in the seasonal distribution of incoming solar radiation across Earth (Otto-Bliesner et al., 2017). Also varying concentrations of well-mixed greenhouse gases are specified in every simulation using ice-core records, although the precise reconstructions used do differ. Those simulations that start in the early Holocene generally incorporate changes in ice-sheet topography and their associated changes in the land-sea mask (Otto-Bliesner et al., 2006; Tian et al., 2022; Hopcroft & Valdes, 2021). Only the simulations with CCSM3 impose meltwater fluxes implied by changes in ice-sheet topography. Reconstructions of volcanic forcing and variations in total solar irradiance introduce forced variability into the simulations, although this has only been done in a single simulation (Dallmeyer et al., 2021). Anthropogenic impacts on global vegetation started with the development of farming in the early Holocene, but became much more substantial approaching the industrial period (Smith & Zeder, 2013). These are incorporated by MPI-ESM using the reconstructions after Hurtt et al. (2011) and Lawrence et al. (2016), but only for the last millennium (850 – 1850 CE).

The zonal-averaged meridional overturning streamfunction in the Atlantic basin is computed for each decade. Given the very weak seasonal cycle in the ocean interior, calendar adjustments to account for variations in the month lengths (Shi et al., 2022) have not been applied. The strength of the AMOC is taken as the maximum streamfunction at 30°N below 500m after Brierley et al. (2020). The computation of the standard deviation of the AMOC at 30°N below 500m is based on a sliding 100-year time window, starting from at earliest 7 ka BP.

Table 1. The ensemble of Holocene transient simulations, their experimental design and primary publication about the individual model description.

Model	**Length of run**	**Forcings**	**Ocean resolution (horizontally, vertically)**	**Reference**
AWI-ESM-2	6ka BP - 0ka BP	orbital, GHG	multi-resolution (finest 25km in polar), 46 levels	Shi et al. (2022)
CCSM3	22ka BP - 0ka BP	orbital, GHG, land-ice, meltwater	longitude 3.6° , latitude varies (finer 0.9° near equator), 25 levels	Otto-Bliesner et al. (2006)
CESM1.2.1	11.5ka - 0.1 ka BP	orbital, GHG, ice-sheets and topography	1° horizontal grid, 60 levels	Tian et al. (2022)
EC-Earth3-veg-LR	8ka - 0 ka BP	orbital, GHG	1° horizontal grid, 75 levels	Zhang et al. (2021)
HadCM3-M2.1d*	10ka - 0 ka BP	orbital, GHG, ice-sheets and sea-level ∗	1.25° × 1.25° , 20 levels	Hopcroft and Valdes (2021)
IPSL-CM5†	6ka - 0 ka BP	orbital, GHG	longitude 2° , latitude 0.5-2° (finer near equator), 31 levels	Braconnot et al. (2019)
KCM	9.5ka - 0 ka BP	orbital, GHG	2° × 2° , 31 levels	Segschneider et al. (2018)
MPI-ESM‡	8ka BP - 0.15 ka BP	orbital, GHG, land-use, ozone, with or without volcanic and solar	1.5° horizontal grid, 41 levels	Bader et al. (2020)

*In this study, we use the simplest of the HadCM3-M2.1d ensemble members, which is the 'xokm' simulation. † This simulation is referred to as 'TR5AS-Vlr01' in Braconnot et al. (2019). ‡ Two simulations of MPI-ESM are used here: SLO50 is the main focus of Bader et al. (2020) and includes volcanic and solar forcing variations, SLO43 does not include them and is only considered as a sensitivity run in Bader et al. (2020).

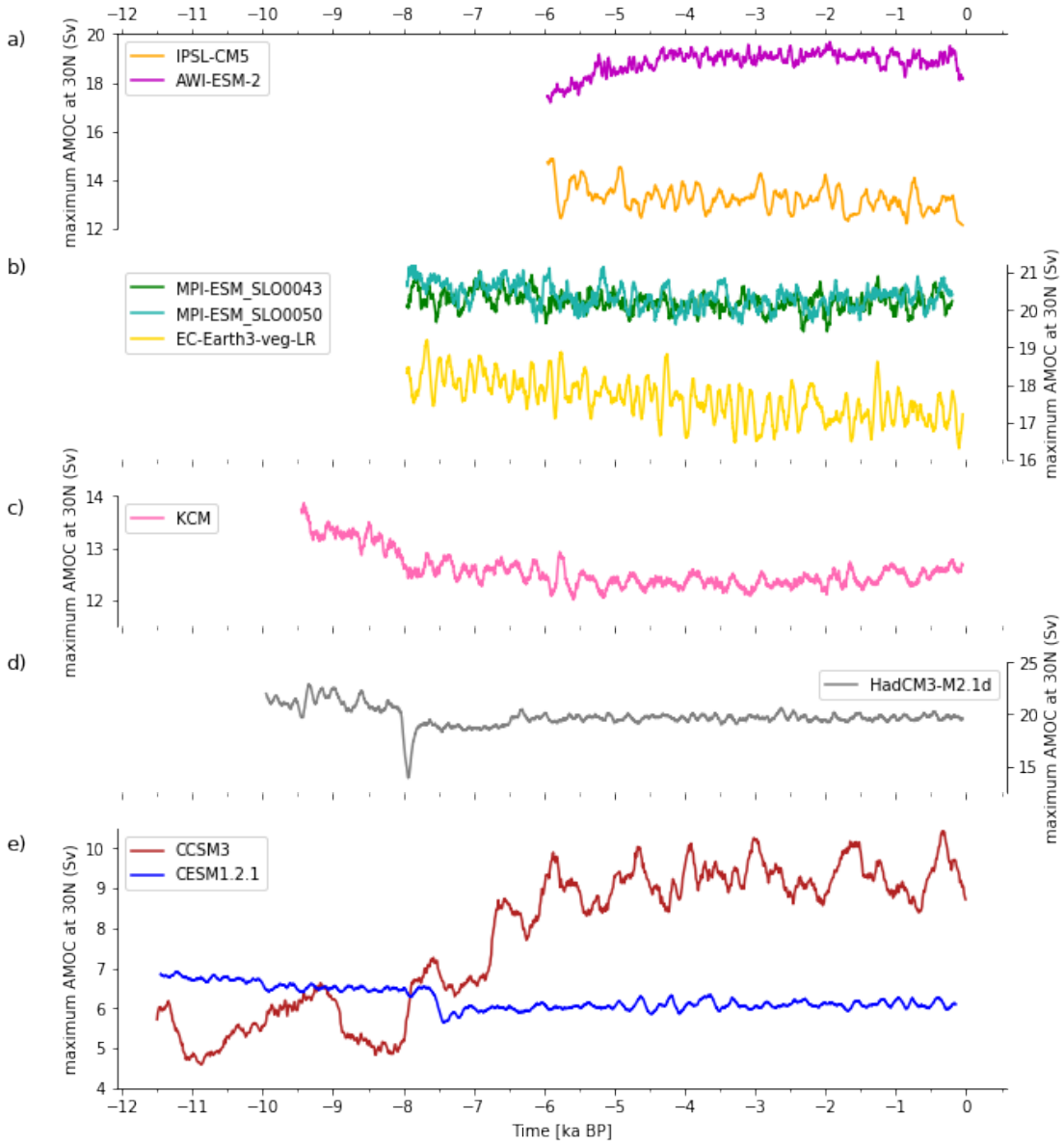

Figure 1. Evolution of the Atlantic Meridional Overturning Circulation (AMOC) in nine climate model simulations. The AMOC strength is tracked by the maximum meridional overturning streamfunction at 30°N below 500m (at a decadal resolution, smoothed by a 100-year running mean). Note the different vertical scales.

3 Results

3.1 Trends in maximum AMOC Strength

The evolution of maximum AMOC strength in each transient simulation is shown in Fig. 1. Changes in AMOC since industrialisation are not captured through a combination of the varying simulation end dates and the 100-year running mean used to smooth the timeseries. Absolute AMOC strength differs substantially between the models (Fig. 1), which is mainly due to the model physics. Two simulations show an overall increasing trend during the past 7,000 years: AWI-ESM-2 (Shi et al., 2022) and CCSM3 (Otto-Bliesner et al., 2006). AWI-ESM-2 sees an enhancement of the AMOC by 10% during 6-4 ka BP, after which the AMOC remains relatively stable and a slight decreasing trend is shown in the late Holocene. The increasing trend in CCSM3 is dominated by the strengthening of AMOC in the early to mid-Holocene, with only a subtle trend from 6 ka BP onwards. Conversely three simulations show an overall decreasing AMOC trend for the maximum AMOC: IPSL-CM5 ($\sim$2 Sv), EC-Earth3-veg-LR ($\sim$1 Sv) and KCM. In KCM there is a decrease of approximately 10% in the early portion, but after roughly 6 ka it remains relatively stable with a marginal increase in the late Holocene (Segschneider et al., 2018). The other simulations do not show any obvious trends in the overall maximum AMOC strength at 30°N through the Holocene (MPI-ESM, HadCM3 and CESM1.2.1). Both transient runs with the MPI-ESM (SLO0043 and SLO0050) do display a slightly higher maximum AMOC strength at 8 to 6 ka BP compared to later periods in the Holocene. In HadCM3, the AMOC strength before and after the 8.2 ka event event remain relatively stable at $\sim$19.5–21 Sv. CESM1.2.1 exhibits a step-change at 7.5 ka BP, but the AMOC is very stable afterwards.

All the simulations that start in the early Holocene (CCSM3, HadCM3, KCM and CESM1.2.1) show stronger changes in AMOC prior to 8 ka than afterwards. The early Holocene saw the 8.2 ka event with a large amount of meltwater entering into the Labrador Sea (e.g. Barber et al., 1999; Matero et al., 2017) through three possible freshwater sources: the sudden discharge of Lake Agassiz, the altered route of the continental freshwater in the North America due to the Laurentide ice sheet melting, and the continuous retreat of Laurentide ice sheet and meltwater release from 9-6 ka BP (Aguiar et al., 2021). However, the different forcings imposed in the simulations (Tab. 1) mean that only CCSM3 responds directly to a changed meltwater flux.

The early Holocene decline in KCM implies an AMOC response to increasing Greenhouse gases, as the lack of a continued trend into the late Holocene rules out an orbital influence (Segschneider et al., 2018). The sudden reduction in AMOC strength in HadCM3 around 8 ka BP arises from the opening of Hudson Bay, when the land sea mask is updated. This connected a large volume of freshwater to the Atlantic and weakened the AMOC for around 250 years. The run with CESM1.2.1 demonstrates an abrupt decrease in AMOC strength by 18% at 7.7 - 7.5 ka BP, after which the AMOC recovered and stabilised, but never returned to the same intensity as that in the early Holocene. The accumulated effect of the rapid retreat of the Laurentide ice sheet from 9 to 7 ka BP (Tian et al., 2022) could be the main cause for the abrupt weakening of AMOC at around 7.7 ka BP in this run.

In conclusion, the transient simulations do not have a consistent message about changes in the overall AMOC strength. Several models simulate changes of roughly $\pm$10%, but these are not of the same sign across models, nor do they exhibit similar temporal behaviours. The few simulations that start in the early Holocene all exhibit stronger changes prior to 6 ka BP than afterwards. This is likely related to the loss of the remnant glacial ice through either meltwater or sea-level changes.

3.2 Trends in spatial structure of streamfunction

There could be robust changes in the the spatial structure of the AMOC, even if there are not consistent changes in its overall strength. We investigate this possibility by mapping

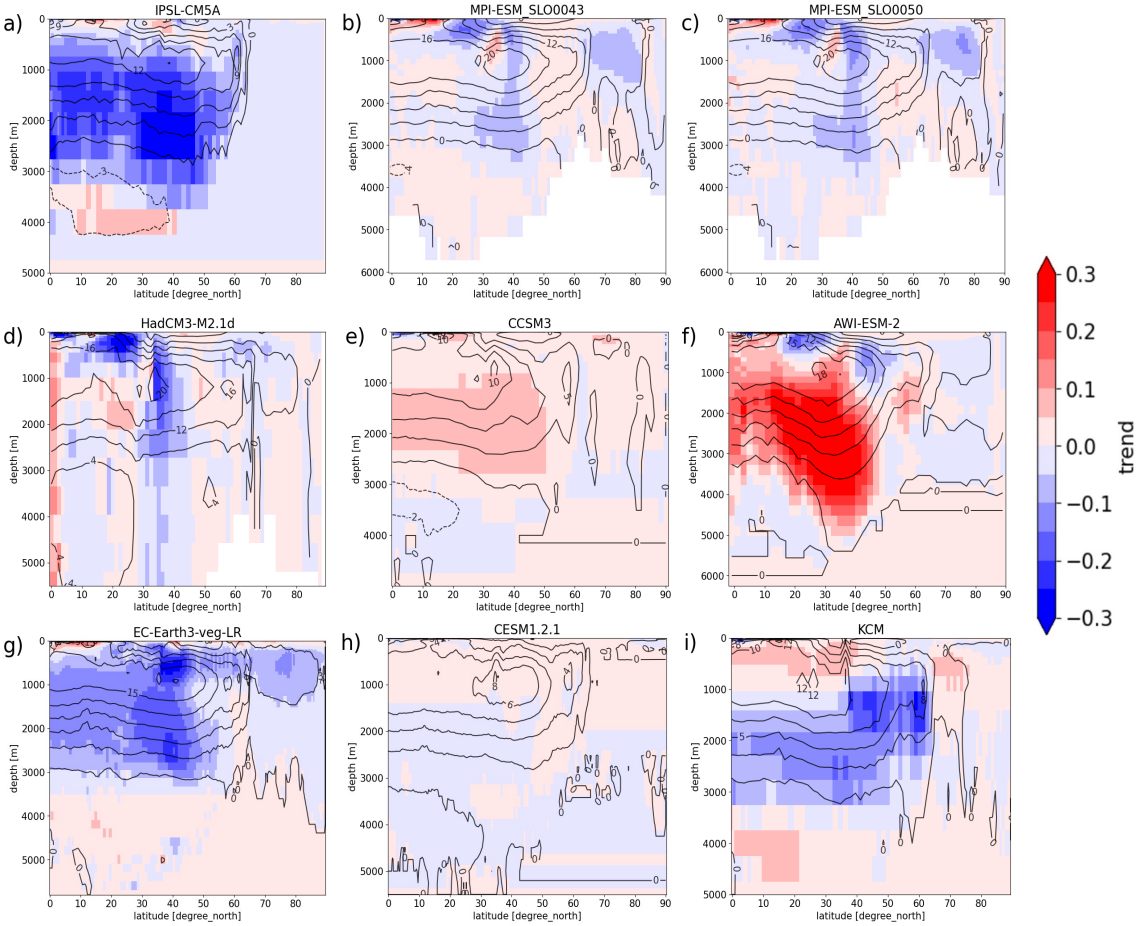

Figure 2. Trend in the meridional streamfunction in the North Atlantic Ocean from 6 ka BP to present (Sv/kyr). The overlaid contours are the mean AMOC spatial pattern at 6-0 ka BP in each model: (a) IPSL-CM5A, (b) MPI-ESM_SLO0043, (c) MPI-ESM_SLO0050, (d) HadCM3-M2.1d, (e) CCSM3, (f) AWI-ESM-2, (g) EC-Earth3-veg-LR, (h) CESM1.2.1, (i) KCM.

the trend in overturning streamfunction at each grid box from 6 ka BP to present (Fig. 2). Two different forms of AMOC change emerge – one showing the whole circulation spinning up (or down) together, and another with a tripole pattern.

Four simulations show a broadly coherent change in terms of in their own streamfunction in the deep southward return flow at 30-50°N, 1,700-3,000m (Fig. 2a, e, g, i; below the maximum AMOC location shown by the overlaid contours). IPSL-CM5 and EC-Earth3-veg-LR show an opposite direction of trend compared to CCSM3, as might be expected given their opposite trends in maximum AMOC strength (Fig. 1). The run with EC-Earth3-veg-LR demonstrates this shift below 3,000 m, but with a similar trend above this level too (Fig. 2g).

A tripole pattern in the mid-latitudes, extending down to ∼1200m, is seen in the simulations by MPI-ESM, HadCM3 and AWI-ESM-2 (Fig. 2b-d,f). This could potentially be associated with changes in the Mediterranean outflow, given the latitude. Ivanovic et al. (2013) explore the impact of the Mediterranean outflow parameterisation in one of the models used here, HadCM3, and demonstrate that it can create changes in AMOC of a similar spatial pattern (Ivanovic et al., 2014). Conversely, Swingedouw et al. (2019) show Mediterranean outflow impacts in IPSL-CM5 that project onto the more-uniform pattern, but then IPSL-CM5 is already in that other set so maybe this is model-specific. The CESM1.2.1 transient run has the weakest trend among all the simulations (Fig. 2h), with almost no trend at any individual sites for the North Atlantic basin from 6-0.1 ka BP. Taken as an ensemble, the simulations do not demonstrate a consistent trend in meridional streamfunction from 6-0 ka BP at any individual locations. Rather they highlight two possible categories of behaviour – either changes in the deep southward return flow (mid-latitudes, 1,700 -3,000 m) or a tripole pattern of change seen in upper subtropics (down to 1,200 m).

3.3 Trends in AMOC variability

The key difference between the two MPI-ESM simulations is the inclusion of externally-forced variability (Bader et al., 2020). This motivates us to explore the AMOC variability throughout the Holocene, which we assess using the standard deviation of the decadally averaged, maximum overturning streamfunction at 30°N calculated over a sliding 100-year time window (Fig. 3). The standard deviation in MPI-ESM SLO0050 is occasionally higher than MPI-ESM SLO043, reflecting the impact of the externally-forced forcing in periods with enhanced volcanic activity (Jungclaus et al., 2014). However, there is clearly a strong role for internal variability, even in the simulation with volcanic and solar forcing. The magnitude of the (internal) variability varies substantially between simulations (Fig. 3). The run with CESM1.2.1 has the smallest magnitude of the internal variability and indicates its simulated AMOC is very stable since 7 ka BP. Meanwhile, the transient runs with CCSM3, IPSL and KCM model also demonstrate relatively smaller magnitude compared to all other runs. Other simulations typically show a magnitude of the internal variability ranging from 1 to 1.5 Sv, with the strongest fluctuations in AWI-ESM2, IPSL and EC-Earth3-veg-LR. The CCSM3 simulation also demonstrates a millennium internal variability for the maximum AMOC at 30°N in the Holocene – this not seen in any other model (Fig. 1), nor in other simulations with the same model (He & Clark, 2022).

None of the simulations show a statistically significant trend in the standard deviations (Fig. 3). Even the largest trend for the standard deviation is less than -0.02 Sv/kyr (in EC-Earth3-veg-LR), which is represents a reduction of under 10% throughout the simulation. Additionally, both small decreasing trends and increasing trends for the internal variability are shown across all the runs, seemingly at random without obvious drivers. Therefore, the internal variability of the AMOC does not change noticeably between 7 ka to present in any of the transient simulations, and there is no consistent message from the ensemble for a trend in the decadal variability of the maximum AMOC at 30°N (Fig. 3).

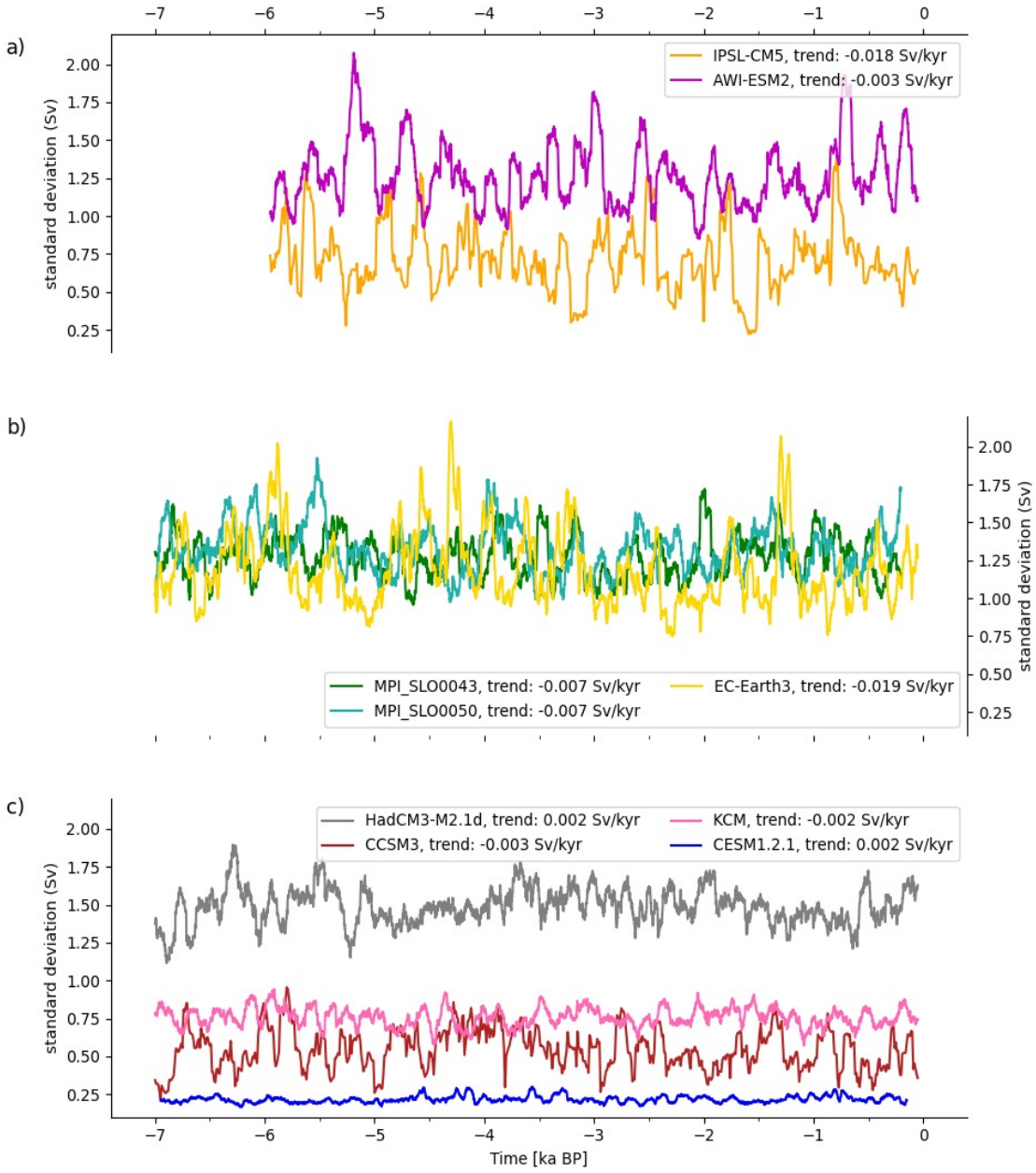

Figure 3. Running standard deviations of the maximum AMOC strength at 30°N below 500m from 7 ka BP to present (based on a sliding 100-year time window).

4 Discussion and conclusions

Overall, there is little support from this ensemble of simulations for changes in AMOC over the past 7,000 years. This is true for trends in overall AMOC strength, and its internal variability. The different experimental set-ups used in the simulations did not appear to play a large role in AMOC evolution since 7,000 years ago, but there were clear consequences from the choice of imposed forcings in the early Holocene. This conclusion fits well with results from PMIP, which performed snapshot simulations for 6,000 years ago. They also found no consistent changes in AMOC strength (Brierley et al., 2020). Combining those mid-Holocene snapshot simulations alongside Last Interglacial simulations suggests that variations in precession would not be expected to alter AMOC (Jiang et al., 2023).

This overriding message of no robust changes in AMOC coming from the ensemble of Holocene transient model simulations is consistent with various reconstructions of the overall AMOC (Fig. 4). These include Pa/Th reconstructions, which have the benefit of (at least potentially) recording the integrated strength of AMOC from a few key sites (Lippold et al., 2019). Multiple independent AMOC reconstructions based upon data assimilation are also now available (Ritz et al., 2013; Osman et al., 2021). Additionally, the winter SST index of Caesar et al. (2018) can be applied to Holocene reconstructions of temperature anomalies (in this instance from Erb et al., 2022) to reconstruct past Holocene AMOC strength. Because the proxy reconstructions are not solely recording November-May SST, the correlation to AMOC is likely slightly weakened and a direct conversion to absolute AMOC changes is not appropriate. Nonetheless this SST fingerprint approach should retain the timing and directions of any AMOC deviations and trends. Collectively these reconstructions also show little change in the AMOC during the mid-to-late Holocene (Fig. 4).

There are, however, some proxy reconstructions do argue for a long-term mid-to-late Holocene decline in AMOC (Ayache et al., 2018; Valley et al., 2022) which at face value would be inconsistent with most of the transient model results presented here (only IPSL-CM5 and EC-Earth3-veg-LR show weakened AMOC since mid-Holocene). Reconstructions can be biased towards individual components of the AMOC, and prior research suggests that a lack of overall AMOC change could be a result of compensation between different AMOC components (Renssen et al., 2005). Furthermore, both the reconstructions derived from surface temperature data assimilation efforts (Fig. 4b,d) show a drop in AMOC over the past 2,000 years. Yet this is not captured by the transient simulations, nor do direct proxy reconstructions show a strong long-term decrease over the last 2,000 years (Rahmstorf et al., 2015; Thornalley et al., 2018).

It has been suggested that the AMOC may play a role in Holocene centennial events, such as the 4.2 ka and 2.8 ka BP events (i.e. Jalali et al., 2019; Denton & Broecker, 2008; Oppo et al., 2003; Keigwin & Boyle, 2000). None of the individual transient simulations capture an event around 4.2 ka or 2.8 ka, (Fig. 1), nor do the assimilation products (Fig. 4), although in the transient ensemble mean the weakest two centennial-scale periods of AMOC occur at ∼4.2 ka and 2.8 ka (Fig. 4). This warrants investigation in further studies, especially as explanations involving volcanic or solar forcing seem unlikely as the majority of simulations do not include them.

In summary, this research suggests that the overall AMOC maintained its strength over the past 7,000 years until the recent changes. The evidence for this conclusion comes from an ensemble of transient simulations using fully-coupled general circulation models, supported by snapshot simulations and data assimilation products. Additionally, we find no consistent trend in the internal variability of the overall AMOC, as the amplitude of decadal variations does not change noticeably between 7 ka to present in any of the simulations. Neither did this research show any support for zonal mean streamfunction trends at particular latitudes or depths. Most paleoceangraphic proxies are more sensitive to reconstructing local oceanographic features rather than the zonally integrated AMOC more local conditions, yet this research did not explore compensation between different components and sources

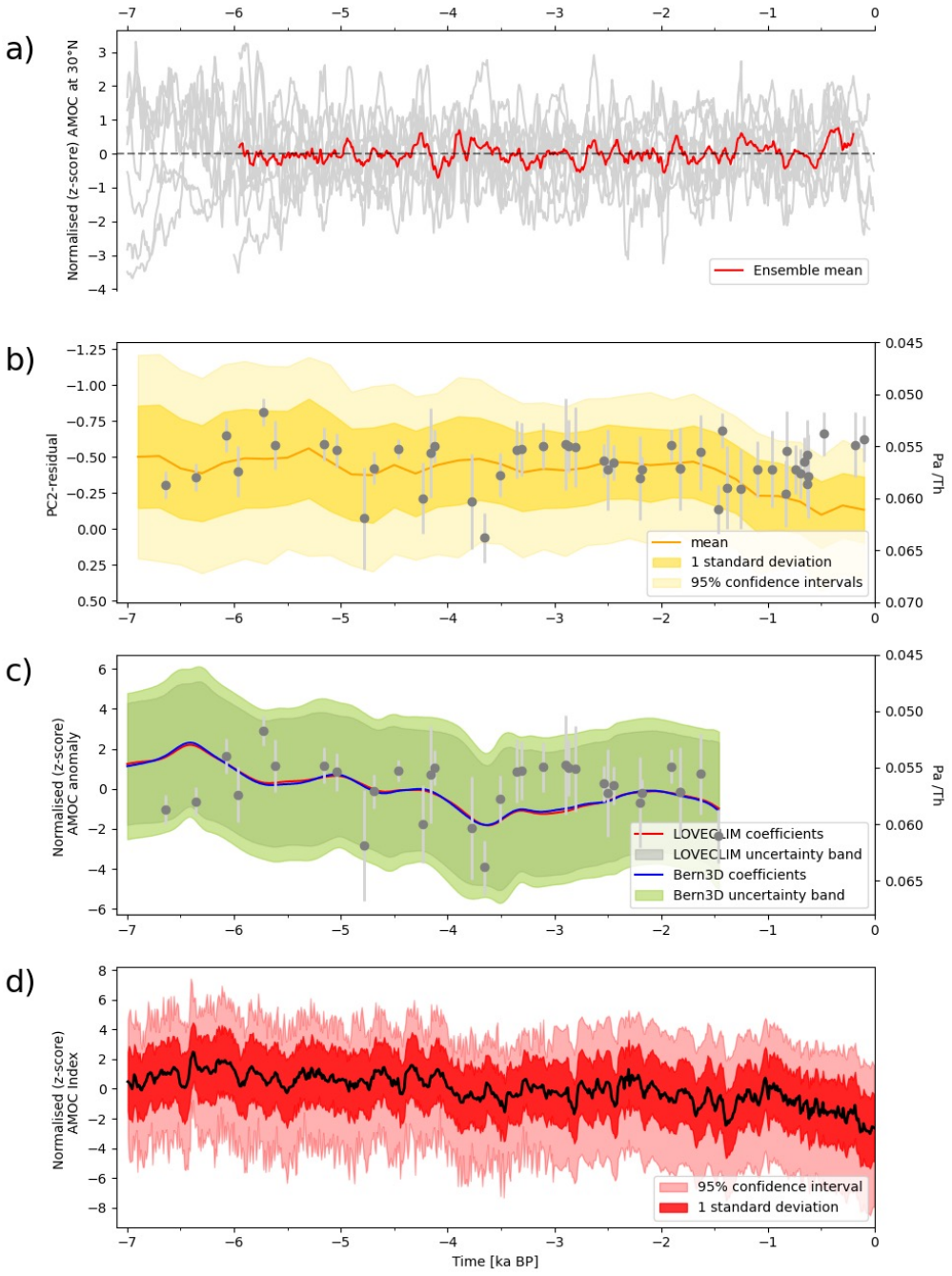

Figure 4. Comparison of AMOC simulations with reconstructions. (a) Ensemble mean of maximum AMOC at 30°N, after each simulation has been standardised by conversion to a z-score over the period 6-0 ka BP. (b) The AMOC reconstruction identified in the reanalysis of Osman et al. (2021). This reanalysis combines marine geochemical data with climate model experiment using proxy system models and data assimilation. Dark and lighter shading on the timeseries indicate $\pm 1\sigma$ and 95% confidence intervals, respectively. (c) AMOC variations reconstructed by Ritz et al. (2013) using data assimilation with priors based on either LOVECLIM or Bern3D simulations. Gray dots are Pa/Th proxy data from Lippold et al. (2019), on the right axis. (d) AMOC variations resulting from applying an annualised SST index (after Caesar et al., 2018) to the surface temperature anomalies reconstructed by Erb et al. (2022) using data assimilation of the temperature12k database (Kaufman et al., 2020).

of North Atlantic deep water. Therefore, further work combining simulations and proxy reconstructions to explore possible compensation between different sub-components of the AMOC may provide useful additional information on future AMOC projections.

Acknowledgments

We would like to thank all the modelling groups who performed the transient simulations and generously made the simulations output freely available. This research has been supported by the UK's Natural Environment Research Council (grant No: NE/S009736/1), the German Federal Ministry of Education and Science (BMBF; 01LP1607A, 01LP1607B, 01LP1609A, 01LP1924B), the German Research Foundation (SFB754, SCH 762/3-1, FO EXC 80/1), the US National Science Foundation (AGS-1903548, AGS-1602223, Cooperative Agreement No. 1852977) and ESC/JAMSTEC computing facilities, National Key Research and Development Program of China (2017YFA0603404), the Strategic Priority Research Program of Chinese Academy of Sciences (XDA20070103), the National Natural Science Foundation of China (41931181 and 42075048), The Swedish Vetenskapsrådet (2013-06476, 2017-04232), European Union's Horizon 2020 (820970), and the French Agence National de Recerche (ANR-15-JCLI-0003-01).

Open Research

The data from the transient runs that used for analysing the AMOC evolution throughout the Holocene in this study are available at Github repository via `https://doi.org/10.5281/zenodo.7499260`.

References

Aguiar, W., Meissner, K. J., Montenegro, A., Prado, L., Wainer, I., Carlson, A. E., & Mata, M. M. (2021). Magnitude of the 8.2 ka event freshwater forcing based on stable isotope modelling and comparison to future Greenland melting. *Scientific reports*, *11*(1), 1–10. doi: 10.1038/s41598-021-84709-5

Argus, D. F., Peltier, W., Drummond, R., & Moore, A. W. (2014). The Antarctica component of postglacial rebound model ICE-6G_C (VM5a) based on GPS positioning, exposure age dating of ice thicknesses, and relative sea level histories. *Geophysical Journal International*, *198*(1), 537–563. doi: 10.1093/gji/ggu140

Ayache, M., Swingedouw, D., Mary, Y., Eynaud, F., & Colin, C. (2018). Multi-centennial variability of the AMOC over the Holocene: A new reconstruction based on multiple proxy-derived SST records. *Global and Planetary Change*, *170*, 172–189. doi: 10.1016/j.gloplacha.2018.08.016

Bader, J., Jungclaus, J., Krivova, N., Lorenz, S., Maycock, A., Raddatz, T., ... Claussen, M. (2020). Global temperature modes shed light on the Holocene temperature conundrum. *Nature Communications*, *11*(1), 1–8. doi: 10.1038/s41467-020-18478-6

Barber, D. C., Dyke, A., Hillaire-Marcel, C., Jennings, A. E., Andrews, J. T., Kerwin, M. W., ... others (1999). Forcing of the cold event of 8,200 years ago by catastrophic drainage of Laurentide lakes. *Nature*, *400*(6742), 344–348. doi: 10.1038/22504

Braconnot, P., Zhu, D., Marti, O., & Servonnat, J. (2019). Strengths and challenges for transient mid-to late Holocene simulations with dynamical vegetation. *Climate of the Past*, *15*(3), 997–1024. doi: 10.5194/cp-15-997-2019

Brierley, C. M., Zhao, A., Harrison, S. P., Braconnot, P., Williams, C. J., Thornalley, D. J., ... Abe-Ouchi, A. (2020). Large-scale features and evaluation of the PMIP4-CMIP6 midHolocene simulations. *Climate of the Past*, *16*(5), 1847–1872. doi: 10.5194/cp-16-1847-2020

Caesar, L., Rahmstorf, S., Robinson, A., Feulner, G., & Saba, V. (2018). Observed fingerprint of a weakening Atlantic Ocean Overturning Circulation. *Nature*, *556*(7700), 191–196. doi: 10.1038/s41586-018-0006-5

Cherchi, A. (2019). Connecting AMOC changes. *Nature Climate Change*, *9*(10), 729–730. doi: 10.1038/s41558-019-0590-x

Crosta, X., Crespin, J., Swingedouw, D., Marti, O., Masson-Delmotte, V., Etourneau, J., ... others (2018). Ocean as the main driver of antarctic ice sheet retreat during the Holocene. *Global and Planetary Change*, *166*, 62–74. doi: 10.1016/j.gloplacha.2018.04.007

Dallmeyer, A., Claussen, M., Lorenz, S. J., Sigl, M., Toohey, M., & Herzschuh, U. (2021). Holocene vegetation transitions and their climatic drivers in MPI-ESM1.2. *Climate of the Past*, *17*(6), 2481–2513. doi: 10.5194/cp-17-2481-2021

Denton, G. H., & Broecker, W. S. (2008). Wobbly ocean conveyor circulation during the Holocene? *Quaternary Science Reviews*, *27*(21-22), 1939–1950. doi: 10.1016/j.quascirev.2008.08.008

Erb, M. P., McKay, N. P., Steiger, N., Dee, S., Hancock, C., Ivanovic, R. F., ... Valdes, P. (2022). Reconstructing Holocene temperatures in time and space using paleoclimate data assimilation. *EGUsphere*, 1–48. doi: 10.5194/cp-18-2599-2022

Fox-Kemper, B., Hewitt, H. T., Xiao, C., Aðalgeirsdóttir, G., Drijfhout, S., Edwards, T. L., ... Y., Y. (2021). Ocean, cryosphere and sea level change [Book Section]. In V. Masson-Delmotte et al. (Eds.), *Climate Change 2021: The Physical Science Basis. Contribution of Working Group I to the Sixth Assessment Report of the Intergovernmental Panel on Climate Change* (chap. 9). Cambridge, United Kingdom and New York, NY, USA: Cambridge University Press. doi: 10.1017/9781009157896.011

He, F. (2011). *Simulating transient climate evolution of the last deglaciation with CCSM3* (Vol. 72) (No. 10).

He, F., & Clark, P. U. (2022). Freshwater forcing of the Atlantic Ocean Overturning Circulation revisited. *Nature Climate Change*, *12*(5), 449–454. doi: 10.1038/s41558-022-01328-2

Hoffmann, S. S., McManus, J. F., & Swank, E. (2018). Evidence for stable Holocene basin-scale overturning circulation despite variable currents along the deep western boundary of the North Atlantic Ocean. *Geophysical Research Letters*, *45*(24), 13,427–13,436. doi: 10.1029/2018GL080187

Hopcroft, P. O., & Valdes, P. J. (2021). Paleoclimate-conditioning reveals a North Africa land–atmosphere tipping point. *Proceedings of the National Academy of Sciences of the United States of America*, *118*(45), e2108783118. doi: 10.1073/pnas.2108783118

Hurtt, G. C., Chini, L. P., Frolking, S., Betts, R., Feddema, J., Fischer, G., ... others (2011). Harmonization of land-use scenarios for the period 1500–2100: 600 years of global gridded annual land-use transitions, wood harvest, and resulting secondary lands. *Climatic Change*, *109*(1), 117–161. doi: 10.1007/s10584-011-0153-2

Ivanovic, R. F., Valdes, P. J., Flecker, R., Gregoire, L. J., & Gutjahr, M. (2013). The parameterisation of Mediterranean–Atlantic water exchange in the Hadley Centre model HadCM3, and its effect on modelled North Atlantic climate. *Ocean Modelling*, *62*, 11–16. doi: 10.1016/j.ocemod.2012.11.002

Ivanovic, R. F., Valdes, P. J., Flecker, R., & Gutjahr, M. (2014). Modelling global-scale climate impacts of the late Miocene Messinian salinity crisis. *Climate of the Past*, *10*(2), 607–622. doi: 10.5194/cp-10-607-2014

Jackson, L. C., Roberts, M. J., Hewitt, H. T., Iovino, D., Koenigk, T., Meccia, V. L., ... Wood, R. A. (2020). Impact of ocean resolution and mean state on the rate of AMOC weakening. *Climate Dynamics*, *55*(7-8), 1711–1732. doi: 10.1007/s00382-020-05345-9

Jalali, B., Sicre, M.-A., Azuara, J., Pellichero, V., & Combourieu-Nebout, N. (2019). Influence of the North Atlantic subpolar gyre circulation on the 4.2 ka BP event. *Climate of the Past*, *15*(2), 701–711. doi: 10.5194/cp-15-701-2019

Jiang, Z., Brierley, C., Thornalley, D., & Sax, S. (2023). No changes in overall amoc strength in interglacial pmip4 time slices. *Climate of the Past*, *19*(1), 107–121. doi: 10.5194/cp-19-107-2023

Jungclaus, J. H., Lohmann, K., & Zanchettin, D. (2014). Enhanced 20th-century heat transfer to the Arctic simulated in the context of climate variations over the last

millennium. *Climate of the Past*, *10*(6), 2201–2213. doi: 10.5194/cp-10-2201-2014

Kageyama, M., Braconnot, P., Harrison, S. P., Haywood, A. M., Jungclaus, J. H., Otto-Bliesner, B. L., ... others (2018). The PMIP4 contribution to CMIP6–Part 1: Overview and over-arching analysis plan. *Geoscientific Model Development*, *11*(3), 1033–1057. doi: 10.5194/gmd-11-1033-2018

Kaufman, D., McKay, N., Routson, C., Erb, M., Davis, B., Heiri, O., ... others (2020). A global database of Holocene paleotemperature records. *Scientific data*, *7*(1), 1–34. doi: 10.1038/s41597-020-0445-3

Keigwin, L., & Boyle, E. (2000). Detecting Holocene changes in thermohaline circulation. *Proceedings of the National Academy of Sciences of the United States of America*, *97*(4), 1343–1346. doi: 10.1073/pnas.97.4.1343

Kobashi, T., Menviel, L., Jeltsch-Thömmes, A., Vinther, B. M., Box, J. E., Muscheler, R., ... others (2017). Volcanic influence on centennial to millennial Holocene Greenland temperature change. *Scientific reports*, *7*(1), 1–10. doi: 10.1038/s41598-017-01451-7

Lawrence, D. M., Hurtt, G. C., Arneth, A., Brovkin, V., Calvin, K. V., Jones, A. D., ... others (2016). The Land Use Model Intercomparison Project (LUMIP) contribution to CMIP6: rationale and experimental design. *Geoscientific Model Development*, *9*(9), 2973–2998. doi: 10.5194/gmd-9-2973-2016

Lippold, J., Pöppelmeier, F., Süfke, F., Gutjahr, M., Goepfert, T. J., Blaser, P., ... Jaccard, S. L. (2019). Constraining the variability of the Atlantic Meridional Overturning Circulation during the Holocene. *Geophysical Research Letters*, *46*(20), 11338–11346. doi: 10.1029/2019gl084988

Lynch-Stieglitz, J., Curry, W. B., & Lund, D. C. (2009). Florida straits density structure and transport over the last 8000 years. *Paleoceanography*, *24*(3), PA3209. doi: 10.1029/2008PA001717

Madec, G., et al. (2008). NEMO ocean engine, version 3.0. *Note du Pôle de modélisation de l'Institut Pierre-Simon Laplace*, *27*, 217. doi: 10.5281/zenodo.3248739

Matero, I., Gregoire, L., Ivanovic, R., Tindall, J., & Haywood, A. (2017). The 8.2 ka cooling event caused by Laurentide ice saddle collapse. *Earth and Planetary Science Letters*, *473*, 205–214. doi: 10.1016/j.epsl.2017.06.011

Mauritsen, T., Bader, J., Becker, T., Behrens, J., Bittner, M., Brokopf, R., ... others (2019). Developments in the MPI-M Earth System Model version 1.2 (MPI-ESM1.2) and its response to increasing CO_2. *Journal of Advances in Modeling Earth Systems*, *11*(4), 998–1038. doi: 10.1029/2018MS001400

Ng, H. C., Robinson, L. F., McManus, J. F., Mohamed, K. J., Jacobel, A. W., Ivanovic, R. F., ... Chen, T. (2018). Coherent deglacial changes in western Atlantic Ocean circulation. *Nature communications*, *9*(1), 1–10. doi: 10.1038/s41467-018-05312-3

Oppo, D. W., McManus, J. F., & Cullen, J. L. (2003). Palaeo-oceanography: Deepwater variability in the Holocene epoch. *Nature*, *422*(6929), 277–278. doi: 10.1038/422277b

Osman, M. B., Tierney, J. E., Zhu, J., Tardif, R., Hakim, G. J., King, J., & Poulsen, C. J. (2021). Globally resolved surface temperatures since the Last Glacial Maximum. *Nature*, *599*(7884), 239–244. doi: 10.31223/x5s31z

Otto-Bliesner, B. L., Braconnot, P., Harrison, S. P., Lunt, D. J., Abe-Ouchi, A., Albani, S., ... Zhang, Q. (2017). The PMIP4 contribution to CMIP6 - Part 2: Two interglacials, scientific objective and experimental design for Holocene and Last Interglacial simulations. *Geoscientific Model Development*, *10*(11), 3979–4003. doi: 10.5194/gmd-10-3979-2017

Otto-Bliesner, B. L., Brady, E. C., Clauzet, G., Tomas, R., Levis, S., & Kothavala, Z. (2006). Last Glacial Maximum and Holocene climate in CCSM3. *Journal of Climate*, *19*(11), 2526–2544. doi: 10.1175/JCLI3748.1

Peltier, W. R., Argus, D., & Drummond, R. (2015). Space geodesy constrains ice age terminal deglaciation: The global ICE-6G_C (VM5a) model. *Journal of Geophysical Research: Solid Earth*, *120*(1), 450–487. doi: 10.1002/2014jb011176

Rahmstorf, S. (2006). Thermohaline ocean circulation. *Encyclopedia of quaternary sciences*, *5*.

Rahmstorf, S., Box, J. E., Feulner, G., Mann, M. E., Robinson, A., Rutherford, S., & Schaffernicht, E. J. (2015). Exceptional twentieth-century slowdown in atlantic ocean overturning circulation. *Nature climate change*, *5*(5), 475–480. doi: 10.1038/nclimate2554

Renssen, H., Goosse, H., & Fichefet, T. (2005). Contrasting trends in north atlantic deep-water formation in the Labrador Sea and Nordic Seas during the Holocene. *Geophysical Research Letters*, *32*(8). doi: 10.1029/2005gl022462

Ritz, S. P., Stocker, T. F., Grimalt, J. O., Menviel, L., & Timmermann, A. (2013). Estimated strength of the Atlantic overturning circulation during the last deglaciation. *Nature geoscience*, *6*(3), 208–212. doi: 10.1038/ngeo1723

Roeckner, E., Bäuml, G., Bonaventura, L., Brokopf, R., Esch, M., Giorgetta, M., ... others (2003). The atmospheric general circulation model ECHAM 5. PART I: Model description. *Max-Planck-Institut für Meteorologie internal report 349*, 144.

Segschneider, J., Schneider, B., & Khon, V. (2018). Climate and marine biogeochemistry during the Holocene from transient model simulations. *Biogeosciences*, *15*(10), 3243–3266. doi: 10.5194/bg-15-3243-2018

Shi, X., & Lohmann, G. (2016). Simulated response of the mid-Holocene Atlantic Ocean Overturning Circulation in ECHAM6-FESOM/MPIOM. *Journal of Geophysical Research: Oceans*, *121*(8), 6444–6469. doi: 10.1002/2015jc011584

Shi, X., Lohmann, G., Sidorenko, D., & Yang, H. (2020). Early-Holocene simulations using different forcings and resolutions in AWI-ESM. *The Holocene*, *30*(7), 996–1015. doi: 10.1177/0959683620908634

Shi, X., Werner, M., Krug, C., Brierley, C. M., Zhao, A., Igbinosa, E., ... others (2022). Calendar effects on surface air temperature and precipitation based on model-ensemble equilibrium and transient simulations from PMIP4 and PACMEDY. *Climate of the Past*, *18*(5), 1047–1070. doi: 10.5194/cp-18-1047-2022

Sidorenko, D., Goessling, H. F., Koldunov, N., Scholz, P., Danilov, S., Barbi, D., ... others (2019). Evaluation of FESOM2.0 coupled to ECHAM6. 3: preindustrial and HighResMIP simulations. *Journal of Advances in Modeling Earth Systems*, *11*(11), 3794–3815. doi: 10.1029/2019MS001696

Smeed, D. A., Josey, S., Beaulieu, C., Johns, W., Moat, B. I., Frajka-Williams, E., ... others (2018). The North Atlantic Ocean is in a state of reduced overturning. *Geophysical Research Letters*, *45*(3), 1527–1533. doi: 10.1002/2017GL076350

Smith, B. D., & Zeder, M. A. (2013). The onset of the anthropocene. *Anthropocene*, *4*, 8–13. doi: 10.1016/j.ancene.2013.05.001

Swingedouw, D., Colin, C., Eynaud, F., Ayache, M., & Zaragosi, S. (2019). Impact of freshwater release in the Mediterranean Sea on the North Atlantic climate. *Climate Dynamics*, *53*(7), 3893–3915. doi: 10.1007/s00382-019-04758-5

Thornalley, D. J., Oppo, D. W., Ortega, P., Robson, J. I., Brierley, C. M., Davis, R., ... others (2018). Anomalously weak Labrador Sea convection and Atlantic overturning during the past 150 years. *Nature*, *556*(7700), 227–230. doi: 0.1038/s41586-018-0007-4

Tian, Z., Jiang, D., Zhang, R., & Su, B. (2022). Transient climate simulations of the Holocene (version 1)–experimental design and boundary conditions. *Geoscientific Model Development*, *15*(11), 4469–4487. doi: 10.5194/gmd-15-4469-2022

Valley, S. G., Lynch-Stieglitz, J., Marchitto, T. M., & Oppo, D. W. (2022). Seawater cadmium in the Florida Straits over the Holocene and implications for upper AMOC variability. *Paleoceanography and Paleoclimatology*, e2021PA004379. doi: 10.1029/2021pa004379

Vieira, L. E. A., Solanki, S. K., Krivova, N. A., & Usoskin, I. (2011). Evolution of the solar irradiance during the Holocene. *Astronomy & Astrophysics*, *531*, A6. doi: 10.1051/0004-6361/201015843

Weijer, W., Cheng, W., Garuba, O. A., Hu, A., & Nadiga, B. T. (2020). CMIP6 models predict significant 21st century decline of the Atlantic Ocean Overturning Circulation. *Geophysical Research Letters*, *47*(12), e2019GL086075. doi: 10.1029/2019GL086075

Zhang, Q., Berntell, E., Axelsson, J., Chen, J., Han, Z., De Nooijer, W., ... others (2021).

493 Simulating the mid-Holocene, last interglacial and mid-Pliocene climate with EC-
494 Earth3-LR. *Geoscientific Model Development*, *14*(2), 1147–1169. doi: 10.5194/gmd
495 -14-1147-2021